IEEE Access
Multidisciplinary ⋮ Rapid Review ⋮ Open Access Journal

Received October 8, 2021, accepted October 18, 2021, date of publication October 29, 2021, date of current version December 2, 2021.

Digital Object Identifier 10.1109/ACCESS.2021.3124218

Compact Planar Tunable Filter With Constant Absolute Bandwidth and Wide-Frequency Tuning Range Using DGS Coupling Structure

YUN LIU[1], LINGYUN LIU[1], CHEN LIANG[1], AND IRFAN MAJID[2], (Senior Member, IEEE)
[1]College of Electronic and Information Engineering, Nanjing University of Aeronautics and Astronautics, Nanjing 210016, China
[2]Department of Aeronautics and Astronautics, Institute of Space Technology, Islamabad 44000, Pakistan

Corresponding author: Yun Liu (lycloud1978@163.com)

This work was supported in part by the National Natural Science Foundation of China under Grant 62071228, in part by the Natural Science Foundation of Jiangsu Province under Grant BK20181290, in part by the Fundamental Research Funds for the Central Universities under Grant NS2019025, and in part by the Open Research Program of Graduate Students' Innovative Laboratory at the Nanjing University of Aeronautics and Astronautics, under Grant kfjj20200404.

ABSTRACT In this study, defected ground structures (DGSs) are applied in the coupling schemes of a planar tunable filter to achieve constant absolute bandwidth (CAB). The filter consists of parallel-coupled quarter-wavelength resonators loaded with varactor diodes, and the DGSs are implemented to enhance the coupling at a certain part. This method enables controlling the ratio between electric coupling and magnetic coupling and makes the total coupling coefficient inversely proportional to frequency, as required to achieve CAB. With the DGSs, the tunable resonators can be equalized to stepped-impedance tunable resonators, which bring wider-frequency tuning range. Moreover, due to the help of the DGS in adjusting the coupling coefficient curve versus frequency, the resonators maintain their universal widths and are coupled at full length. Thus, the tunable filter is as compact as a traditional combline filter. Meanwhile, each external coupling scheme contains a series capacitor and a short-ended stub that is parallel coupled to the first or last resonator, resulting in external Q factor being proportional to frequency. A second-order tunable filter is designed and measured, and a wide tuning range from 0.63 GHz to 1.09 GHz together with a constant bandwidth of 65±4 MHz are achieved. Besides, a transmission zero generated by coupling zero of the DGS-loaded coupling structure can be observed at the high stopband. The total dimension of the filter is 0.05 λ_g * 0.15λ_g, which is more compact than solutions with partial-length coupling schemes. Owing to the simple structures of the resonators and coupling schemes, the filter solution has the potential to design high-order tunable filters with CAB, and a compact fourth-order tunable filter with ABC is given with simulation results.

INDEX TERMS Tunable filter, defected ground structure, constant absolute bandwidth.

I. INTRODUCTION

Modern wireless communication systems increasingly need reconfigurable RF front ends in which electrically tunable filters are key components. In many applications, constant absolute bandwidths (CABs) are desirable for tunable filters if the telecommunication mode and specifications need to be unchanged when the frequency varies. In the literature, tunable filters with CABs are commonly realized using half-wavelength tunable resonators [1]–[3] and quarter-wavelength tunable resonators [4]–[8]; the latter are more compact in dimension and have wider tuning range of frequency. To achieve CAB, the internal coupling coefficients between resonators should be inversely proportional to frequency, and this condition is achieved in several ways. Partial-length coupling schemes are developed in [1]–[4], [7], providing a suitable ratio between electric and magnetic coupling and needed curves of coupling coefficient versus center frequency. However, the filters are not compact as tunable filters with full-length parallel coupling schemes [5], [6], [8] because the uncoupled parts should be departed with a distance. To meet the requirements of CAB, stepped impedance resonators [5] and series LC-loaded resonators [8] are adopted to adjust the electric and magnetic couplings, and

The associate editor coordinating the review of this manuscript and approving it for publication was Giovanni Angiulli.

inductive coupling is enhanced by introducing a meander connecting line between resonators [6]. Of course, CAB can be achieved by providing tunability on coupling coefficients with varactor diodes [9], but many more varactor diodes are required with greatly increased complexity in circuit and tuning.

Wide tuning range of center frequency is also an important consideration for practical applications, and this has not been sufficiently studied in the past [10]–[12]. In [10], the wide tuning range is achieved with stepped-impedance quarter-wavelength resonators, but the circuit is not compact due to the adoption of a partial-length coupling scheme. A shorter transmission line and a series inductor are used to obtain a large tuning range of filter frequency, however, the bandwidth cannot be kept constant [11]. In [12], ultra-wide frequency tuning range is achieved by using filter-bank technology in which three tunable filters are stacked in a multilayered structure. However, the solution is complex and lossy, and the absolute bandwidth is not constant.

Many of the published tunable filters [1], [2], [4], [7], [9], [10] with CABs have a filter order of two, which is too low to realize high out-of-band rejection. To obtain a high-order tunable filter with CAB, we need both the two-side coupling coefficients of an inner resonator to be inversely proportional to frequency. However, this requirement cannot be easily satisfied because the resonator can hardly provide enough design freedoms to two-side coupling schemes simultaneously, especially when the resonators are not axisymmetric in structure.

Defected ground structures (DGSs) have been used in the design of filters [13]–[15]. DGSs applied in coupling schemes can ensure tight input/output couplings between either a port and the multi-mode resonator, thus realizing ultra-wideband bandpass filters [13]. DGSs can also act as resonating elements on the ground to realize bandstop filters [14] and dual-band bandpass filters [15].

In this study, a compact tunable combline filter with CAB and wide tuning range is proposed by loading DGSs under the resonators and under the parallel coupling schemes. With the DGSs loaded, the electric coupling and magnetic coupling can be easily adjusted, resulting in the total coupling coefficient becoming inversely proportional to frequency, which satisfies the need to realize CAB. Moreover, the DGSs cause the resonators to become stepped-impedance tunable resonators, and the frequency tuning range is efficiently expanded. As the DGSs on the ground layer provide more design freedom in adjusting the coupling coefficient slopes, simple universal-width tunable resonators are parallel coupled, and the filter order can be continuously increased. Unlike many bulky tunable filters using partial-length couplings, the proposed tunable filter has compact dimensions because the resonators are coupled in full length with no redundant area.

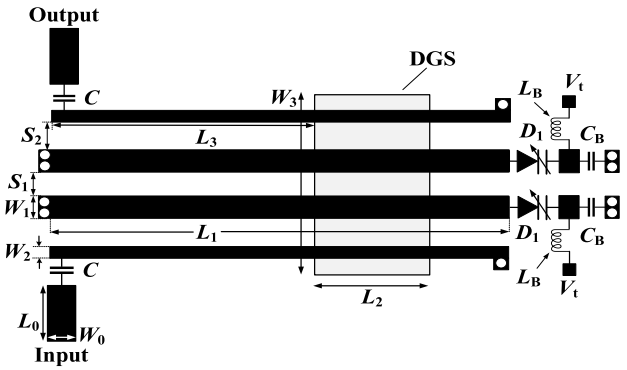

FIGURE 1. Structure of proposed tunable filter.

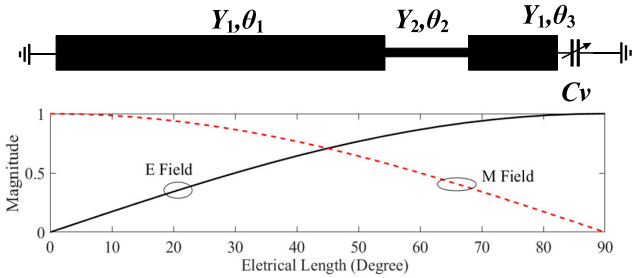

FIGURE 2. Equivalent circuit and field distributions of DGS-loaded tunable resonator.

II. STRUCTURE AND THEORY OF FILTER

Fig. 1 shows the circuit of a proposed second-order tunable combline filter with constant absolute bandwidth. Here, the two quarter-wavelength resonators are loaded with varactor diodes at the open ends for electrical tuning of resonance frequencies, whereas each diode is biased with a shunt capacitor C_B and a series inductor L_B. A defected DGS is loaded below the filter to provide constant bandwidth. As the DGS introduced can greatly reduce the distributive capacitance of the transmission line and achieve high characteristic impedance conveniently, each resonator can be regarded as a stepped-impedance resonator with an equivalent circuit shown in Fig. 2. A wider frequency tuning range can be achieved [11] compared with that of the varactor-loaded universal-impedance resonator. Approximately, the electric and magnetic field have sinusoidal and cosine distributions along the resonator, respectively, as shown in Fig. 2. The resonator has the strongest electric field at the end loaded with the varactor and the strongest magnetic field at the grounded end [16].

As shown in Fig. 3(a), the two resonators are parallel coupled, and the rectangular DGS of certain width, length, and position is implemented to tune the electric and magnetic couplings to achieve coupling coefficient, which is inversely proportional to the resonating frequency, thereby satisfying the requirement of constant absolute bandwidth [4]. When the DGS is arranged close to the grounded end with the strongest magnetic field, the magnetic coupling is increased. On the

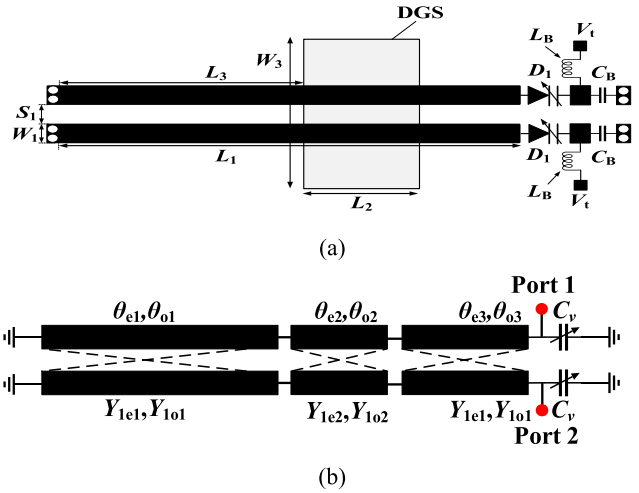

FIGURE 3. Structure and equivalent circuit of coupled resonators with DGS: (a) structure and (b) equivalent circuit.

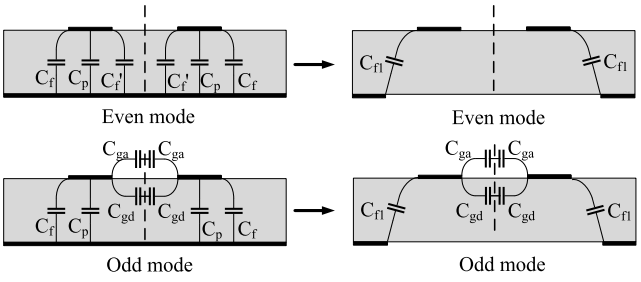

FIGURE 4. Comparison of microstrip coupled line to DGS-loaded coupled line: (a) microstrip coupled line and (b) DGS-loaded microstrip coupled line.

contrary, if the DGS is close to the end loaded varactor, the electric coupling is increased. By changing the position of the DGS, the ratio between electric and magnetic couplings can be adjusted; thus, the slope of the frequency-dependent coupling coefficient is tuned.

Fig. 3(b) shows the equivalent circuit of Fig. 3(a), containing three sections of parallel coupled lines, and the section loaded with DGS has increased even- and odd-mode characteristic impedances because of the decreased distributive capacitance between the strips and the ground, as shown in Fig. 4.

A microstrip coupled line has characteristic impedances expressed as

$$\begin{cases} Z_{e1} = \dfrac{1}{v_{pe1}\left(C_f + C_p + C_{f'}\right)} \\ Z_{o1} = \dfrac{1}{v_{po1}\left(C_f + C_p + C_{f'} + C_{gd} + C_{ga}\right)}, \end{cases} \tag{1}$$

where C_{f1}, C_p, $C_{f1'}$, C_{gd}, and C_{ga} are distributed capacitances, and v_{pe1}, v_{po1}, v_{pe2} and v_{po2} are phase velocities of even/odd modes.

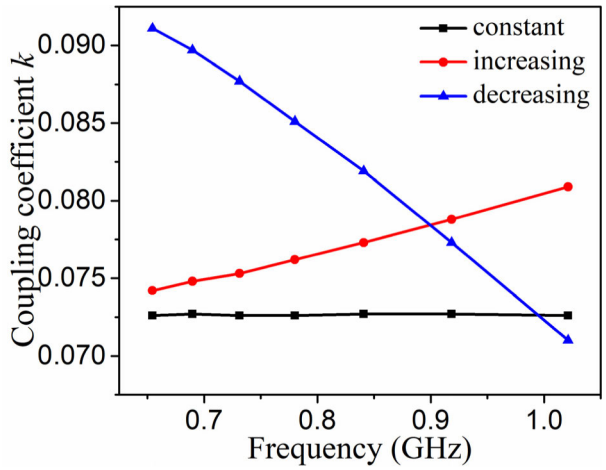

FIGURE 5. Three k curves with different slopes (calculated with formulas).

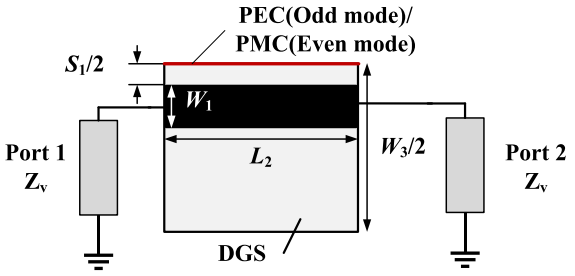

FIGURE 6. Two-port simulation model for evaluating even- and odd-mode characteristic impedances for coupled line section with DGS.

The characteristic impedance changes when the DGS is implemented as follows:

$$\begin{cases} Z_{e2} = \dfrac{1}{v_{pe2}C_{f1}} \\ Z_{o2} = \dfrac{1}{v_{po2}\left(C_{f1} + C_{gd} + C_{ga}\right)}. \end{cases} \tag{2}$$

Considering that v_{pe1}, v_{po1}, v_{pe2}, and v_{po2} are close in value, we have

$$\frac{Z_{2e}}{Z_{2o}} > \frac{Z_{1e}}{Z_{1o}}. \tag{3}$$

This condition means that the DGS enhances the field coupling where the DGS is implemented, regardless of whether it is electric or magnetic.

From Fig. 3(b), we can deduce the even- and odd-mode input admittance of the two-port network as follows [4]:

$$Y_{ine} = j\omega C_v + Y_{re}, \tag{4}$$

$$Y_{ino} = j\omega C_v + Y_{ro}. \tag{5}$$

Here, C_v is the series equivalent capacitance value of the varactor diode D_1 and

$$Y_{re} = Y_{1e1}\frac{\frac{-jY_{1e2}(Y_{1e1}-Y_{1e2}\tan\theta_{e1}\tan\theta_{e2})}{Y_{1e2}\tan\theta_{e1}+Y_{1e1}\tan\theta_{e2}} + jY_{1e1}\tan\theta_{e3}}{Y_{1e1} + \frac{Y_{1e2}(Y_{1e1}-Y_{1e2}\tan\theta_{e1}\tan\theta_{e2})}{Y_{1e2}\tan\theta_{e1}+Y_{1e1}\tan\theta_{e2}}\tan\theta_{e3}}, \tag{6}$$

$$Y_{ro} = Y_{1o1}\frac{\frac{-jY_{1o2}(Y_{1o1}-Y_{1o2}\tan\theta_{o1}\tan\theta_{o2})}{Y_{1o2}\tan\theta_{o1}+Y_{1o1}\tan\theta_{o2}} + jY_{1o1}\tan\theta_{o3}}{Y_{1o1} + \frac{Y_{1o2}(Y_{1o1}-Y_{1o2}\tan\theta_{o1}\tan\theta_{o2})}{Y_{1o2}\tan\theta_{o1}+Y_{1o1}\tan\theta_{o2}}\tan\theta_{o3}} \quad (7)$$

The Y matrix of the two-port network in Fig. 2(b) can then be given as

$$Y = \begin{pmatrix} (Y_{ine}+Y_{ino})/2 & (Y_{ine}-Y_{ino})/2 \\ (Y_{ine}-Y_{ino})/2 & (Y_{ine}+Y_{ino})/2 \end{pmatrix}, \quad (8)$$

$$\mathrm{Im}[Y_{11}(\omega_0)] = 0, \quad (9)$$

$$k = \frac{\mathrm{Im}[Y_{12}(\omega_0)]}{b}, \quad (10)$$

$$b = \frac{\omega_0}{2}\frac{\partial \mathrm{Im}[Y_{11}(\omega_0)]}{\partial\omega}|_{\omega=\omega_0}. \quad (11)$$

The introduced DGS structure provides three design freedoms, which are L_2, L_3, and W_3. Here, L_2 and W_3 are the length and width of DGS, and larger W_3 results in larger odd- and even-mode characteristic impedances, which can bring larger coupling for the part. When L_3 is increasing, the DGS section becomes closer to the loaded varactors, introducing larger electric coupling. By contrast, if L_3 is decreasing, then the magnetic coupling increases. Using the formulas, we can compute the coupling coefficient curves. Fig. 5 presents three different curves, which are constant, increasing, and decreasing monotonously, respectively. This situation occurs when the DGS is close to the center part, grounded end, and varactor diodes. Evidently, the curve slope can be tuned by the position and dimensions of the DGS. All the dimensions, characteristic impedances, and electrical lengths of the three cases are listed in Table 1. The even- and odd-mode characteristic impedances of the DGS-loaded section are obtained by conducting two-port simulations [17] with varied port impedance Z_v if the symmetric plane is set to be PMC for even mode and PEC for odd mode, as presented in Fig. 4. Good matching happens when the port impedance is equal to the characteristic impedance, and then the electrical length can be read out from the phase response of S_{21}.

For practical design, we can simulate and calculate the coupling coefficient by using the eigenmode solver of HFSS [17], and the following classic formula can be used:

$$|k| = \frac{f_h^2 - f_l^2}{f_h^2 + f_l^2}, \quad (12)$$

where f_h and f_l are even and odd resonating frequencies when two resonators are coupled. In HFSS simulation, each varactor is simply modeled as a series combination of a tunable capacitor and a resistor by applying lumped RLC boundaries [17].

Figs. 7 (a, b, c) provide simulated curves of k when the main parameters of the DGS are changing. Here, L_2 and W_3 are length and width of the DGS, and L_3 is the distance from grounded end to the DGS. By increasing L_2 and W_3, one can efficiently increase the coupling coefficient over the tuning range of frequency, and adjust the coupling coefficient slope to a certain extent.

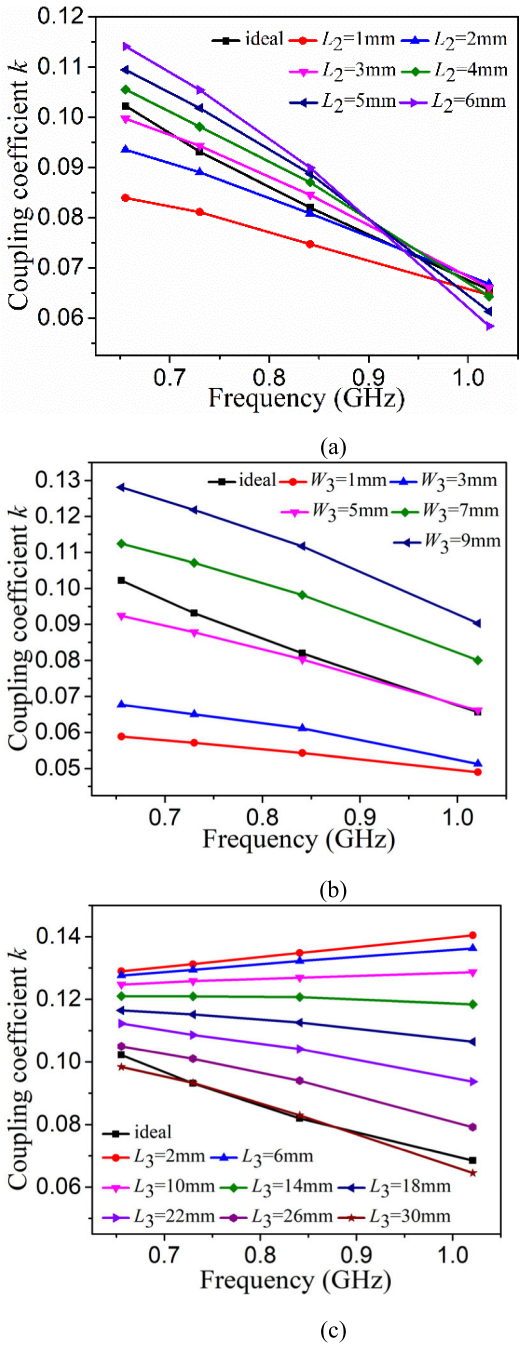

FIGURE 7. Variation of k curves when DGS dimensions change: a) k vs. L_2(L_1 = 35, L_3 = 27.5, W_3 = 6); b) k vs. W_3(L_1 = 35, L_2 = 3, L_3 = 27.5.); c) k vs. L_3(L_1 = 35, L_2 = 3, W_3 = 6). All figures are in mm.

We can observe that the k curve slope is mainly dominated by L_3. When L_3 is smaller and DGS is closer to the grounded end, the magnetic coupling is larger, and the k curve slope is more positive. On the contrary, a negative slope happens when the DGS is closer to the end loaded with the varactor.

By tuning the three parameters and the distance S_1, the practical k curve can approach an ideal k curve, which is inversely proportional to frequency, as required for realizing the tunable filter with CAB.

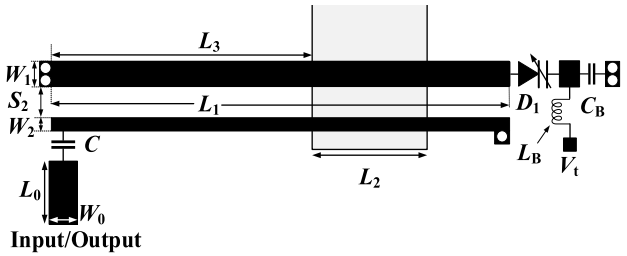

FIGURE 8. Input/output coupling circuit for tunable filter with CAB.

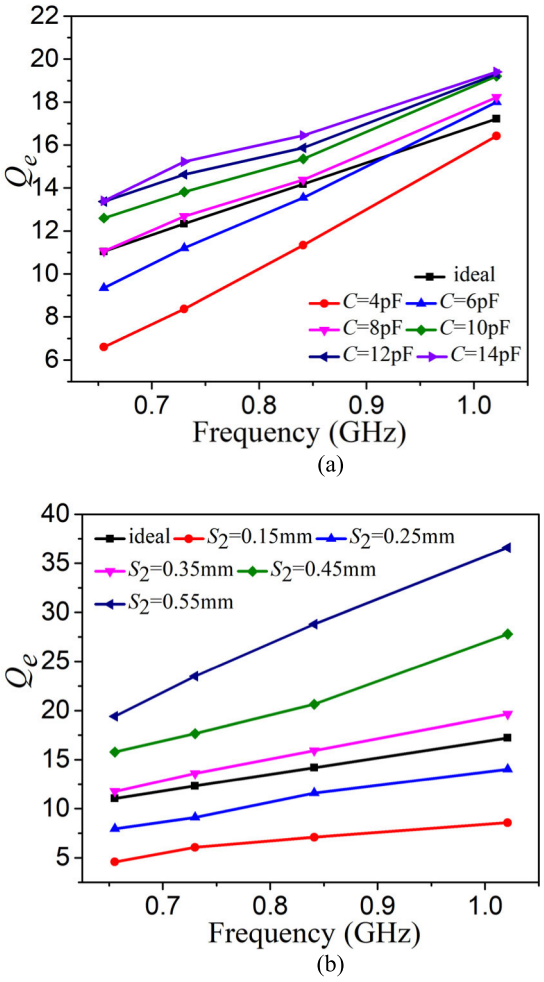

FIGURE 9. Circuit and simulated results of a fourth-order tunable filter with CAB: a) circuit and b) simulated S parameters.

Fig. 8 shows the input/output coupling circuit for achieving CAB [4], where a parallel coupling scheme is adopted, and the coupling line is connected to the port through a capacitor and grounded at the end. For accurate simulation of the external coupling, the effect of DGS is also counted, as the DGS also extends to the area of the input/output coupling circuit. The circuit provides two design freedoms, S_2 and C, which can be used to adjust both the value and the curve slope of external quality factor Q_e, which represents the strength of external coupling.

Similarly, we can compute Q_e after conducting a one-port simulation of Fig. 8, and the formula is given as follows:

$$Q_e = f_0/|f_{+90^\circ} - f_{-90^\circ}|, \tag{13}$$

where f_0 is the resonant frequency, and f_{+90° and f_{-90° are the two frequencies with $+90^\circ$ and -90° phase responses of S_{11}. To achieve CAB, the Q_e should be proportional to the frequency across the frequency tuning range.

Fig. 9 presents the curves of Q_e when the values of S_2 and C are changing. As can be observed, the Q_e value can be effectively adjusted by tuning S_2, while the curve slope is mainly affected by capacitance C.

A design procedure for the tunable filter with CAB can be given as follows:

1) With the specified frequency tuning range, constant bandwidth and out-band rejection, one can decide the filter order and select a suitable prototype lowpass filter with suitable insertion loss ripple.
2) The ideal k curves for inner couplings and the ideal Q_e curve for input/output couplings are computed using synthesis formulas for classic microwave filters [18].
3) Initial parameters of microstrip quarter-wave length resonator are given, and a coupled resonator circuit model is constructed by implementing DGS, as shown in Fig. 3. By optimizing the parameters of DGS, we can achieve needed k curves, which are inversely proportional to frequency.
4) External coupling circuits are constructed, as shown in Fig. 8, and the required Q_e curve is achieved, which is proportional to frequency, by optimizing parameters such as C and S_2.
5) A full circuit of the tunable filter similar to that in Fig. 1 is constructed. Full-wave simulation and optimization is performed for optimal results.

III. FILTER IMPLEMENTATION AND RESULTS

Based on the proposed circuit in Fig. 1 and the design method, a tunable bandpass filter was designed with a constant bandwidth of 65 MHz and a frequency tuning range from 0.68 GHz to 1.05 GHz. The ideal k_{12} and Q_e of the filter are calculated by the constant absolute bandwidth formulas (14) and (15), and the corresponding curves are shown in Figs. 3 and 5, respectively.

$$k_{12} = \frac{ABW}{f_0\sqrt{g_1 g_2}}, \tag{14}$$

$$Q_{e1} = \frac{f_0 g_0 g_1}{ABW} \quad Q_{e2} = \frac{f_0 g_2 g_3}{ABW}. \tag{15}$$

Here, the element values of the lowpass prototype filter are: $g_0 = 1$, $g_1 = 0.8431$, $g_2 = 0.622$ $g_3 = 1.3554$. The design of the filter is based on a Rogers substrate with a P/N of 4003 C. The relative dielectric constant is 3.38 and the thickness is 0.508 mm.

The final dimensions (in mm) of the filter are given as $L_0 = 3.4$, $W_0 = 1.1$, $L_1 = 35$, $W_1 = 1$, $L_2 = 3$, $W_2 =$

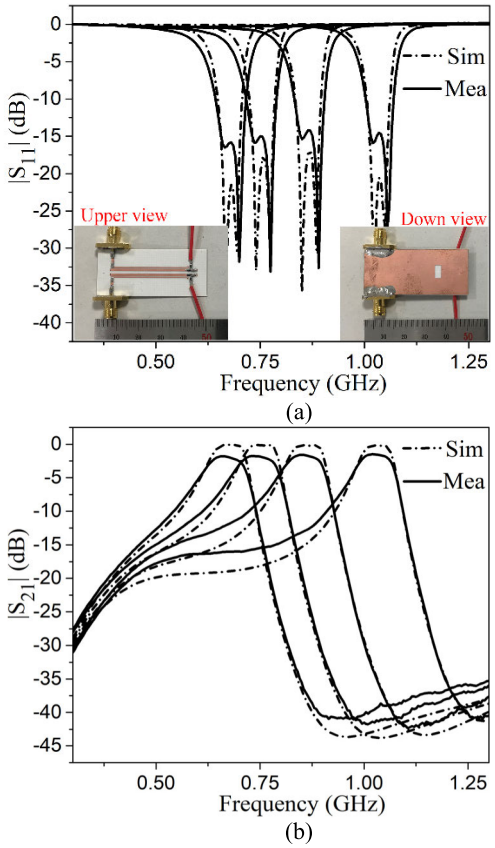

FIGURE 10. Compared S parameters and photographs of the tunable filter: a) S_{11} and b) S_{21}.

0.5, $W_3 = 6$, $S_1 = 1.2$, $S_2 = 0.33$, and $L_3 = 27.5$. The capacitance C for input/output couplings is 8 pF. Varactor diodes with a P/N of SMV1408-040LF (Skyworks) are chosen with capacitance value ranging from 0.95 pF to 4.08 pF when the biasing voltage is tuned from 0 V to 30 V. Additionally, the biasing elements have values of $C_B = 100$ pF and $L_B = 100$ nH.

Fig. 10 compares the simulated and measured S parameter responses of this filter. The overall size of the filter is $0.15\lambda_g \times 0.05\lambda_g$, where λ_g is the guided wavelength at 0.68 GHz. The simulated and measured results are in good agreement.

The simulation is conducted with HFSS, and the measurement is conducted by using an Agilent N5230C network analyzer. The photographs are also given.

When the reverse bias voltage changes from 0.2–25 V, we can obtain a bandpass filtering response with the center frequency shifting from 0.68 to 1.05 GHz, and the frequency tuning range is 54%. Over the entire frequency range, the 1 dB bandwidth is within 65 ± 4 MHz. The lowest insertion loss within the passband is 1.7–1.8 dB and the return loss remains better than 15 dB, which are acceptable for many practical applications.

The S_{21} response is asymmetric with higher rejection at the upper stopband, and a maximum rejection of 40 dB can be observed at the frequency approximately 200 MHz away from the passband due to mixed electric and magnetic coupling, provided by the DGS-loaded parallel coupling structure.

A fourth-order filter is also designed as shown in Fig. 11 (a). The filter is symmetric in structure and three sepa-

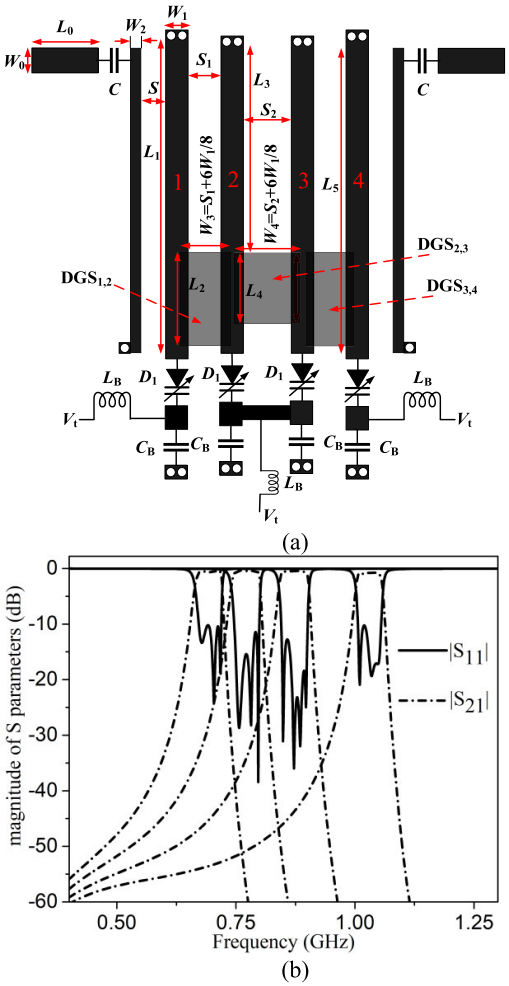

FIGURE 11. Compared S parameters and photographs of tunable filter: a) S_{11} and b) S_{21}.

TABLE 1. Comparison with previous works.

	Freq (GHz)	TR (%)	BW (MHz)	IL (dB)	Size ($\lambda_g \times \lambda_g$)	Order	Tuning Elements
[1]	0.65-0.96	47	80±3.5	1.2-1.5	0.12×0.12	2	Varactors
[4]	0.92-1.34	45	43±3	1.9-2.9	0.11×0.06	2	Varactors
[7]	1.55-2.04	31	72±3	1.9-2	0.23×0.15	2	RF-MEMS
[8]	1.7-2.2	29	98±6	1.6-2	0.49×0.37	2	Varactors
[12]	0.1-0.61	500	Not const.	4	6.25*5 (cm^2)	2	Varactors Filter bank
Present study	0.68-1.05 0.7-1.03	54 47	65±4 65±3	1.7-1.8 <0.8 (Sim.)	0.15×0.05 0.15×0.10	2 4	Varactors

rate DGSs are used to achieve coupling coefficients inversely proportional to frequency. The filter applies the same substrate, varactors, and biasing circuits used in the second-order tunable filter. After circuit optimization, the simulated S parameters are presented in Fig. 11(b). The center frequency can be tuned from 0.7 GHz to 1.03 GHz when the capacitance is tuned from 4 pF to 1 pF. Within the frequency tuning range, the return loss is better than 10 dB and the 1 dB bandwidth is kept as 65 $\pm$ 3 MHz. As the filter order is higher, the out-of-band rejection is much higher. All the dimensions and parameters are listed as follows: $L_0 = 3.4$ mm; $W_0 = 1.1$ mm; $L_1 = 35$ mm; $W_1 = 1$ mm; $L_2 = 8$ mm; $W_2 = 0.5$ mm; $L_3 = 25$ mm; $W_3 = 2.05$ mm; $S = 0.3$ mm; $S_1 = 1.3$ mm; $S_2 = 1.7$ mm; $L_4 = 6$ mm; $W_4 = 2.45$ mm; $L_5 = 35.3$ mm; $C = 10$ pF; $L_B = 100$ nH; $C_B = 100$ pF.

Table 1 presents a performance comparison of this work and several previously published tunable filters. The results show that the proposed filter exhibits advanced features such as compact dimensions and wider frequency-tuning range.

Commonly tunable filters with CABs are larger in dimension than traditional fixed filters because redundant circuit areas always exist between resonators when partial-length coupling schemes are used. However, the proposed tunable filters can have compact dimensions similar to those of traditional combline filters. This is partly due to the adoption of quarter-wavelength resonators, and partly by the full-length coupling schemes between resonators, in which all the resonators are arranged closely without redundant circuit areas.

The wider frequency tuning range is obtained because the resonators are in fact stepped impedance resonators. Although the resonators are universal in width, they have higher characteristic impedances where the DGSs are loaded. As DGSs are responsible for obtaining the CAB, the resonators and coupling schemes can be simplified, which is why high-order tunable filter can be designed conveniently.

IV. CONCLUSION

This paper presented a novel tunable bandpass filter with a constant absolute bandwidth by adopting full-length parallel coupling scheme loaded with DGS. The partial-length DGS can easily adjust the ratio between electric and magnetic couplings. The total coupling coefficient can be inversely proportional to the frequency, which helps achieve CAB. Furthermore, the partially loaded DGSs cause the universal-width $\lambda/4$ resonators to be stepped-impedance resonators in nature. Thus, a broader frequency tuning range is achieved after varactor capacitors are applied. As the resonators have universal width and the full-length parallel coupling scheme is implemented, high-order filters with constant absolute bandwidths can be obtained with dimensions as traditional combline filters.

REFERENCES

[1] X. Y. Zhang, Q. Xue, C. H. Chan, and B.-J. Hu, "Low-loss frequency-agile bandpass filters with controllable bandwidth and suppressed second harmonic," *IEEE Trans. Microw. Theory Techn.*, vol. 58, no. 6, pp. 1557–1564, Jun. 2010, doi: 10.1109/TMTT.2010.2048250.

[2] W.-J. Zhou and J.-X. Chen, "High-selectivity tunable balanced bandpass filter with constant absolute bandwidth," *IEEE Trans. Circuits Syst. II, Exp. Briefs*, vol. 64, no. 8, pp. 917–921, Aug. 2017, doi: 10.1109/TCSII.2016.2621120.

[3] M. Ohira, S. Hashimoto, Z. Ma, and X. Wang, "Coupling-matrix-based systematic design of single-DC-bias-controlled microstrip higher order tunable bandpass filters with constant absolute bandwidth and transmission zeros," *IEEE Trans. Microw. Theory Techn.*, vol. 67, no. 1, pp. 118–128, Jan. 2019, doi: 10.1109/TMTT.2018.2873366.

[4] S. J. Park and G. M. Rebeiz, "Low-loss two-pole tunable filters with three different predefined bandwidth characteristics," *IEEE Trans. Microw. Theory Techn.*, vol. 56, no. 5, pp. 1137–1148, May 2008, doi: 10.1109/TMTT.2008.921638.

[5] B.-W. Kim and S.-W. Yun, "Varactor-tuned combline bandpass filter using step-impedance microstrip lines," *IEEE Trans. Microw. Theory Techn.*, vol. 52, no. 4, pp. 1279–1283, Apr. 2004, doi: 10.1109/TMTT.2004.825626.

[6] N. Zahirovic, S. Fouladi, R. R. Mansour, and M. Yu, "Tunable suspended substrate stripline filters with constant bandwidth," in *IEEE MTT-S Int. Microw. Symp. Dig.*, Jun. 2011, p. 1–4, doi: 10.1109/MWSYM.2011.5972931.

[7] M. A. El-Tanani and G. M. Rebeiz, "High-performance 1.5–2.5-GHz RF-MEMS tunable filters for wireless applications," *IEEE Trans. Microw. Theory Techn.*, vol. 58, no. 6, pp. 1629–1637, Jun. 2010, doi: 10.1109/TMTT.2010.2049166.

[8] X.-G. Wang, Y.-H. Cho, and S.-W. Yun, "A tunable combline bandpass filter loaded with series resonator," *IEEE Trans. Microw. Theory Techn.*, vol. 60, no. 6, pp. 1569–1576, Jun. 2012, doi: 10.1109/TMTT.2012.2189123.

[9] M. Jung and B.-W. Min, "A widely tunable compact bandpass filter based on a switched varactor-tuned resonator," *IEEE Access*, vol. 7, pp. 95178–95185, 2019, doi: 10.1109/ACCESS.2019.2929746.

[10] W. Qin, J. Cai, Y.-L. Li, and J.-X. Chen, "Wideband tunable bandpass filter using optimized varactor-loaded SIRs," *IEEE Microw. Wireless Compon. Lett.*, vol. 27, no. 9, pp. 812–814, Sep. 2017, doi: 10.1109/LMWC.2017.2734848.

[11] T. Lim, A. Anand, J. Chen, X. Liu, and Y. Lee, "Design method for tunable planar bandpass filters with single-bias control and wide tunable frequency range," *IEEE Trans. Circuits Syst. II, Exp. Briefs*, vol. 68, no. 8, pp. 221–225, Jan. 2021, doi: 10.1109/TCSII.2020.3004614.

[12] J. S. Sun, N. Kaneda, Y. Baeyens, T. Itoh, and Y.-K. Chen, "Multilayer planar tunable filter with very wide tuning bandwidth," *IEEE Trans. Microw. Theory Techn.*, vol. 59, no. 11, pp. 2864–2871, Nov. 2011, doi: 10.1109/TMTT.2011.2163201.

[13] H. Wang and L. Zhu, "Aperture-backed microstrip line multiple-mode resonator for design of a novel UWB bandpass filter," in *Proc. Asia–Pacific Microw. Conf.*, Dec. 2005, p. 4.

[14] A. B. Abdel-Rahman, A. K. Verma, A. Boutejdar, and A. S. Omar, "Control of bandstop response of Hi-Lo microstrip low-pass filter using slot in ground plane," *IEEE Trans. Microw. Theory Techn.*, vol. 52, no. 3, pp. 1008–1013, Mar. 2004.

[15] J. Shi, J. X. Chen, and Q. Xue, "A quasi-elliptic function dual-band bandpass filter stacking spiral-shaped CPW defected ground structure and back-side coupled strip lines," *IEEE Microw. Wireless Compon. Lett.*, vol. 17, no. 6, pp. 430–432, Jun. 2007.

[16] D. M. Pozar, *Microwave Engineering*. Beijing, China: Publishing House of Electronics, 2004.

[17] *Ansys HFSS: Best-in-Class 3D High Frequency Electromagnetic Simulation Software*. Accessed: Aug. 1, 2021. [Online]. Available: http://www.ansys.com/Products/Electronics/ANSYS-HFSS

[18] R. W. Wyndrum, "Microwave filters, impedance-matching networks, and coupling structures," *Proc. IEEE*, vol. 53, no. 7, p. 766, Jul. 1964, doi: 10.1109/PROC.1965.4048.

YUN LIU was born in Dongtai, Jiangsu, China, in 1978. He received the B.S. and M.S. degrees in radio physics from Nanjing University, Nanjing, China, in 2000 and 2004, respectively, and the Ph.D. degree from the State Key Laboratory of Millimeter Waves, Southeast University, Nanjing, in 2009. In 2009, he joined the Nanjing University of Aeronautics and Astronautics, Nanjing, where he is currently an Associate Professor. From September 2016 to September 2017, he was a Visiting Professor with the Department of Electrical and Computer Engineering, University of Florida, Gainesville, FL, USA. His current research interests include microwave filters and passive components.

LINGYUN LIU was born in Shaoyang, Hunan, China, in 1998. She received the B.S. degree in electrical information engineering from the Nanjing University of Aeronautics and Astronautics, Nanjing, China, in 2019. Her current research interests include microwave filters and phase shifter.

CHEN LIANG received the B.S. and M.S. degrees in electrical engineering from the Nanjing University of Aeronautics and Astronautics, Nanjing, China, in 2017, and 2021, respectively. His main research interests include microwave filters and other passive components.

IRFAN MAJID (Senior Member, IEEE) received the B.E. degree in avionics engineering (major RF/microwave engineering) from the NED University of Engineering and Technology, Karachi, Pakistan, in 1988, and the M.S. degree in avionics engineering (major RF/microwave engineering) from the National University of Sciences and Technology, Islamabad, Pakistan, in 2004. He was with the Pakistan Air Force from 1988 to 2001 and from 2014 to 2017, where he has been a part of various engineering research and development projects. He was an Associate Professor with the Faculty of Avionics Engineering, National University of Sciences and Technology, Risalpur, Pakistan, from 2002 to 2008. He was with the Centers of Excellence in Science and Applied Technologies, Islamabad, from 2008 to 2014. Since September 2017, he has been an Assistant Professor with the Department of Avionics Engineering, Institute of Space Technology, Islambad. His current research interests include avionics system design and aircraft electromagnetic compatibility analysis.